

# Nonlinear Framework for Speech Bandwidth Extension

Tarikul Islam Tamiti, Nursad Mamun, and Anomadarsi Barua, George Mason University, USA

## Abstract

Recovering high-frequency components lost to bandwidth constraints is crucial for applications ranging from telecommunications to high-fidelity audio on limited resources. We introduce NDSI-BWE, a new adversarial Band Width Extension (BWE) framework that leverage four new discriminators inspired by non-linear dynamical system to capture diverse temporal behaviors: a Multi-Resolution Lyapunov Discriminator (MRLD) for determining sensitivity to initial conditions by capturing deterministic chaos, a Multi-Scale Recurrence Discriminator (MS-RD) for self-similar recurrence dynamics, a Multi-Scale Detrended Fractal Analysis Discriminator (MSDFA) for long range slow variant scale invariant relationship, a Multi-Resolution Poincaré Plot Discriminator (MR-PPD) for capturing hidden latent space relationship, a Multi-Period Discriminator (MPD) for cyclical patterns, a Multi-Resolution Amplitude Discriminator (MRAD) and Multi-Resolution Phase Discriminator (MRPD) for capturing intricate amplitude-phase transition statistics. By using depth-wise convolution at the core of the convolutional block with in each discriminators, NDSI-BWE attains an eight-times parameter reduction. These seven discriminators guide a complex-valued ConformerNeXt based generator with a dual stream Lattice-Net based architecture for simultaneous refinement of magnitude and phase. The generator leverage the transformer based conformer’s global dependency modeling and ConvNeXt block’s local temporal modeling capability. Across six objective evaluation metrics and subjective based texts comprises of five human judges, NDSI-BWE establishes a new SoTA in BWE.

## 1 Introduction

However, despite these advancements, current deep learning models often struggles to capture the inherent non-linear and chaotic properties of speech,

such as deterministic chaos, complicated relationship between low and high frequency components, and state-space complexity. The production of speech is fundamentally non-linear, characterized by irregular oscillations and bifurcations, which results into deterministic chaos that conventional linear or purely data-driven models fail to capture mostly. This limitation results in perceptual artifacts such as sibilance, oversmoothing, aliasing, and temporal blurring, which adversely affects the perceived quality of the reconstructed speech.

Another new paradigm in BWE is the usage of Diffusion Models. Generative Adversarial Networks (GAN) shows promising realistic high-frequency reconstruction. But due to the inherent limitation of traditional discriminators that failed to capture subtle nuances of audios which fail generators to produce crispier audios. This paper addresses this limitation by leveraging chaos theory and nonlinear dynamical system concepts. By designing discriminators to capture one particular type of non-linear dynamics, which subsequently results into generator being particularly sensitive to one distinct classes of signal behaviors. These discriminators combinedly captures repeating structures, chaotic divergence, sensitive state-space transitions, and hidden dynamical states, respectively.

Nonlinear dynamical theory is essential in BWE due to the inherent non-linear nature of human speech production. Speech signals exhibit complex behaviors, including turbulence and irregular oscillations arising from the nonlinear interaction of airflow and vocal tract structures. These nonlinearities can not be represented by linear models or conventional GANs using traditional discriminators, which relies primarily on capturing linear or mildly linear dependencies.

Moreover, chaotic dynamics play a crucial role in accurately modeling the temporal evolution of speech signals. Deterministic chaos, characterized by sensitivity to initial conditions and unpre-

dicted yet deterministic evolution, frequently happen in speech. Traditional CNN-based discriminators without explicit modeling of this deterministic chaos fail to capture this intricate subtleties. Adding nonlinear dynamics ensures temporal complexities and sensitive dependencies are effectively captured and embedded in the reconstructed speech. Non-linear theories enables discriminators to explicitly differentiate between naturally occurring chaotic structures and artificial smoothness or periodicity of the synthesized by the naive generator. The introduction of nonlinear discriminators not only improves the perceptual realism of reconstructed audio but also significantly reduces sibilance and oversmoothing, which ensures that the generated bandwidth extended audio has a more natural sounding experience.

Lastly, non-linear dynamical approaches facilitate a deeper understanding and modeling of hidden states and phase-space transitions in audio. Traditional spectral-domain discriminators overlook critical dynamical relationships in state-space trajectories, which are very important for understanding audio perception. Non-linear dynamical discriminators, directly address this shortcoming, effectively capturing and preserving the dynamical complexity inherent in speech signals. Integrating non-linear dynamical discriminators within the NDSI-BWE generator framework yields a compact, efficient architecture which enables discriminators to address the challenges posed by speech’s chaotic nature side by side achieves superior suppression of non-perceptual artifacts and generate more high-fidelity audios.

In summary, this paper’s contributions are introduction of non-linear dynamical systems inspired discriminators capable of jointly capturing chaotic, periodic, recurrent, and hidden dynamical audio patterns. We design a meticulously curated complex-valued dual-stream NDSI-BWE framework for simultaneous improvement of magnitude and phase spectrograms. Comprehensive objective and subjective evaluation over a wide variety metrics demonstrate that our approach, bring a new research paradigm in BWE while setting new benchmark with fewer number of parameter, faster inference speed and enhanced perceptual quality.

The reminder of the paper is structured as follows. Section II reviews related works in BWE and non-linear dynamical systems. Section III presents the detailed architecture of the proposed generator and discriminators. Section IV outlines our ex-

perimental setup and evaluation metrics. Results, including objective and subjective analyses, are discussed in Section V. Finally section VI concludes the paper, discusses the limitations and suggests future research directions.

## 2 Related Work

**Traditional Signal-Processing Methods.** Early BWE approaches predicted high-frequency spectral envelopes using source-filter modelling, codebook mapping, and statistical techniques. Key contributions include the iterative Griffin–Lim algorithm for phase reconstruction (?), LPC-based extensions with codebook mapping to infer spectral bands (?), and GMM/HMM mapping methods for envelope prediction. Matrix-factorization techniques further explored low-rank spectral modeling, but all suffered from over-smoothed outputs and limited adaptability.

**Neural-Network-Based Approaches.** With deep learning, neural models vastly outperformed traditional methods. Early work applied fully-connected DNNs and CNNs to predict wideband magnitude spectra or directly generate time-domain waveforms in end-to-end architectures. Waveform-based models (e.g., the Nu-Wave series) bypass spectrogram inversion, while spectrogram-based methods predict complex spectra, often with dual-stream amplitude/phase networks (e.g., AP-BWE) and multi-resolution discriminators to mitigate blurring. Hybrid approaches operate in subbands (e.g., UBGAN uses PQMF) or combine time- and frequency-domain blocks for best of both worlds.

## 3 Overall Architecture

The overview of the proposed architecture is illustrated in Fig. 1.

### 3.1 Generator Architecture

Because of the necessity of phase along with amplitude (Yin et al., 2020; Lu et al., 2024b), the generator of our NDSI-BWE parallelly receives both the amplitude and phase cues from the two computed synchronized feature maps. The magnitude spectrogram is obtained by taking the logarithm of the absolute value of the Short-Time Fourier Transform (STFT), and the phase spectrogram is obtained by taking the angle of the STFT. We define the narrow-band magnitude and phase spectrograms by  $\mathbf{M}_{\text{nb}}$  and  $\Phi_{\text{nb}}$ , respectively, in Eqn. 1.

$$\mathbf{M}_{\text{nb}} \in \mathbb{R}^{B \times F \times T}, \quad \Phi_{\text{nb}} \in \mathbb{R}^{B \times F \times T} \quad (1)$$

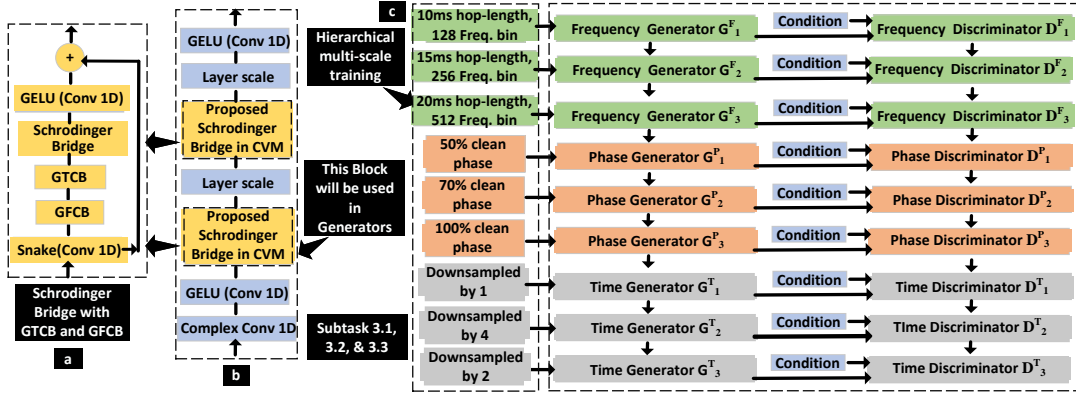


Figure 1: It has complex encoders, decoders, complex skip blocks, CGAB.

where  $B$  is the batch size,  $F$  is the number of frequency bins ( $F = \frac{n_{FFT}}{2} + 1$ ), and  $T$  is the number of time frames. Its forward pass consists of three main stages:

**a) Parallel Post-Processing:** The generator initially processes the narrow-band magnitude and phase in two separate streams and merge them into a common latent space at the end, harmonizing heterogeneous inputs into a unified projection.

**b) Lattice Block Interaction:** The Lattice block (Luo et al., 2020) ensures continuous controlled mixing of magnitude and phase streams that enables explicit exchange of information, reweighing each stream’s contribution, and faster convergence. Although the model could get faster inference for the absence of this mixing, however, the absence of the mixing results in error accumulation in the streams, ”muffled” artifacts in the reconstructed wideband audio signal, and unstable training. Therefore, we apply two successive one-dimensional Lattice blocks (**Lattice1D**), each of which interleaves the magnitude and phase streams via criss-cross connections by learnable scalars, denoted by  $\alpha_1, \alpha_2, \beta_1$ , and  $\beta_2$  in Fig. 1. These scalars perform as a gating function by controlling the strength of cross-stream injection. These scalars are trained end-to-end and dynamically learns ”where” and ”how-much” cross-stream interactions are required.

Within each Lattice block, we insert a new block named **ConformerNeXt**. We design ConformerNeXt by replacing the standard Conformer’s (Gulati et al., 2020) convolutional sub-module with a ConvNeXt (Liu et al., 2022) block. This replacement significantly enhances the model’s capacity by combining ConvNeXt’s powerful hierarchical spatial feature extraction with Conformer’s global self-attention. Our proposed ConformerNeXt takes two inputs instead of one, as opposed to (Luo et al.,

2020). Moreover, the pre- and post-processing convolutions used in the original Lattice Nets in (Luo et al., 2020) are omitted. This variation provides the best choice for the inter-stream connectivity.

As there are two Lattice blocks and each contains one ConformerNeXt per stream, the full generator employs a total of four ConformerNeXt with cross-stream residual connections. After trying out various combinations of connections and the number of ConformerNeXt, we find out that this design provides the best trade-off between performance and reduced number of parameters.

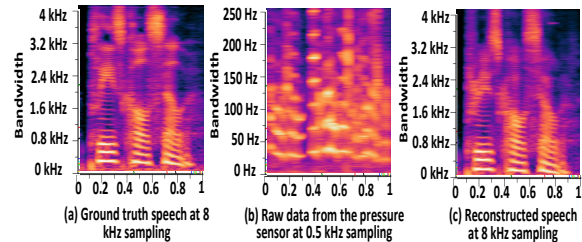


Figure 2: Dummy.

**c) Residual Prediction and Synthesis:** After the final Lattice stage, separate output heads estimate the wideband residuals by passing the output of the final Lattice block through Layer Normalization (LN) and Linear Projection (Proj) blocks. Inspired by (Lu et al., 2024b), the magnitude branch outputs a log-magnitude residual that is added to the narrow-band input to isolate and recover only missing high-frequency information rather than remodeling the entire spectrum.

Moreover, previous works (Yin et al., 2020) show that due to the noisy nature of the phase, it is very difficult to estimate the phase directly. To overcome these difficulties in direct phase estimation, the phase branch’s output is fed into two Feed-Forward Neural Networks, for predicting ”pseudo-real” and ”pseudo-imaginary” residuals, shown in Eqn. 2. Finally, the wide-band phase is recovered by the ’arctan2’ function, by stacking the magnitude and phase branch complex spectrogram is

generated, whose Inverse Short Time Fourier Transform (ISTFT) is used for the reconstruction of the wideband audio.

$$\begin{aligned} R &= \text{Proj}_r(\text{LN}(\Phi^{(4)})) \\ I &= \text{Proj}_i(\text{LN}(\Phi^{(4)})) \end{aligned} \quad (2)$$

$$\Phi_{\text{wb}} = \text{atan2}(I, R)$$

$$\mathbf{C}_{\text{wb}} = e^{\mathbf{M}_{\text{wb}}} (\cos \Phi_{\text{wb}} + i \sin \Phi_{\text{wb}}) \quad (3)$$

### 3.2 Chaos-Informed Nonlinear Discriminator

Speech production is fundamentally a *non-linear dynamical process characterized by deterministic chaos* (Little et al., 2007). Traditional GAN discriminators (Tian et al., 2020), (Donahue et al., 2018), (Kumar et al., 2019) typically minimize the distance between reconstructed and original speech based on raw waveforms or spectrogram slices, but fail to detect those nonlinear chaotic cues. Therefore, generators produce over-smoothed and dull spectra (Cao et al., 2024). In this paper, we design two chaos-inspired nonlinear discriminators - Lyapunov and Detrended Fluctuation. This is the first time that these two discriminators have been proposed to be included with complex-valued generative models to explore the chaotic study of audio reconstruction. They analyze long-range and hidden formant trajectories and micro-transients across equally spaced windows, output chaos-aware feature maps, and penalize any mismatch in sub-harmonic richness. Our approach results in a 40x reduction in discriminator size, 0.5x fewer parameters, and overall more realistic acoustics (see Sections 4.6, 4.4, & 4.8) with less over-smoothed spectra compared to SOTA models (Lu et al., 2024b,a).

**a) Multi-Resolution Lyapunov Discriminator (MRLD):** We introduce Lyapunov Exponents (LE) (Oseledec, 1968; Wolf et al., 1985) to capture the rapid, nonlinear fluctuations and sensitivity to initial conditions in speech that spectrogram-based losses overlook. The LE is a measure of nonlinear dynamics used to quantify the rate of separation of infinitesimally close trajectories. Therefore, MRLD penalizes the mismatches in the Lyapunov spectra of real and generated signals and drives the generator to reproduce authentic deterministic chaotic behavior, yielding more lifelike speech.

A pseudo-algorithm 1 is provided to explain how MRLD is implemented. MRLD divides each waveform into non-overlapping windows  $w \in \{64, 128, 256, 512, 1024\}$ , computes local LE via delay-embedding and nearest-neighbor divergence, and map each segment to a single divergence rate

(lines 1-7). Then, MRLD feeds these exponent maps into a five-layer depthwise-separable 1D CNN with kernel size 5 (stride 2 for the first four layers, final kernel 3, 235 K parameters) to discriminate real versus generated dynamics.

---

#### Algorithm 1: Pseudo-code of MRLD

---

**Require:** Raw waveform  $x$ , window sizes

$$\mathcal{W} = \{64, 128, 256, 512, 1024\}$$

**Ensure:** Predicted label  $y \in \{\text{real}, \text{generated}\}$

- 1:  $\mathcal{F} \leftarrow \square$  {Initialize feature list}
  - 2: **for all**  $w \in \mathcal{W}$  **do**
  - 3:   **for all** segment  $x_i^w$  in  $x$  with window size  $w$  **do**
  - 4:     Delay-embed  $x_i^w$  into vectors  $\{y_j\}$  using dimension  $d$ , delay  $\tau$
  - 5:     Compute 
$$\lambda_i^w = \text{Avg}_j \left[ \frac{1}{\Delta} \log \left( \frac{\|y_{j+\Delta} - y_{j'+\Delta}\| + \epsilon}{\|y_j - y_{j'}\| + \epsilon} \right) \right]$$
  - 6:     Append  $\lambda_i^w$  to  $\mathcal{F}$
  - 7:   **end for**
  - 8: **end for**
  - 9: Normalize and reshape  $\mathcal{F}$  for CNN input
  - 10:  $y \leftarrow \text{CNN}_{\text{MRLD}}(\mathcal{F})$
  - 11: **return**  $y$
- 

**b) Multi-Scale Detrended Fluctuation Analysis Discriminator (MSDFA):** We introduce Detrended Fluctuation Analysis (DFA) to quantify fractal-like, long-range temporal correlations that conventional spectrogram losses overlook. Therefore, by computing how root-mean-square fluctuations  $F(n)$  grow with window size, MSDFA supervises the generator to ensure natural-sounding dynamics across syllabic, phonemic, and sub-phonemic scales. If omitted, the adversarial framework leads to muffled prosody even when amplitude and phase discriminators are present.

A pseudo-algorithm 2 is provided to explain how MSDFA is implemented. We integrate classical DFA at  $n \in \{100, 200, 300, 500, 600\}$  samples, tile each  $F(n)$  into a fixed  $S \times S$  map, and feed the resulting tensor into a five-layer depthwise-separable 2-D CNN (batch-norm + LeakyReLU) whose adversarial loss back-propagates through the tiling, making MSDFA a light ( $\approx 247\text{K}$  parameters) yet powerful plug-in discriminator for BWE problems.

**c) Multi-Resolution Amplitude & Phase Discriminators (MRAD & MRPD):** In addition to MRLD and MSDFA, we also use MRAD and MRPD in our adversarial framework. MRAD ensures that amplitude transients are captured in different granularities. MRPD stabilizes group delay

and explores harmonic-phase relationships. We refer to (Lu et al., 2024b) for the implementation details of MRAD and MRPD. In contrast to (Lu et al., 2024b), we use three resolutions, such as frequency bins = [512, 128, 512], hop sizes = [1024, 256, 1024], and window lengths = [2048, 512, 2048]. Each resolution is fed to a 5-layer 2D CNN (varied kernels/strides, weight-norm, LeakyReLU).

---

**Algorithm 2:** Pseudo-code of MSDFA

---

**Require:** Input waveform  $x(t)$ , scales  $\mathcal{N} = \{100, 200, 300, 500, 600\}$   
**Ensure:** Real/fake score  $y \in \mathbb{R}$

- 1:  $\mathcal{F} \leftarrow \emptyset$
- 2: **for all**  $n \in \mathcal{N}$  **do**
- 3:   Compute DFA fluctuation  $F(n)$  on  $x(t)$
- 4:   Tile  $F(n)$  into fixed-size map  $M^{(n)} \in \mathbb{R}^{S \times S}$  and Append  $M^{(n)}$  to  $\mathcal{F}$
- 5: **end for**
- 6:  $T \leftarrow \text{stack}(\mathcal{F}) \in \mathbb{R}^{S \times S \times 5}$
- 7:  $y \leftarrow \text{CNN}_{\text{MSDFA}}(T)$  {5-layer depthwise-separable CNN}
- 8: **return**  $y$

---

## 4 Comprehensive Result Analysis

### 4.1 Evaluation Metrics

We assess the fidelity, intelligibility and perceptual quality of the bandwidth-extended signals using six complementary objectives: Log-Spectral Distance (LSD) to quantify fine-grained spectral deviations; Short-Time Objective Intelligibility (STOI) to evaluate speech intelligibility; Perceptual Evaluation of Speech Quality (PESQ) to predict overall quality in line with human judgments; Scale-Invariant SDR (SI-SDR) as a general distortion metric agnostic to amplitude scaling; Scale-Invariant SNR (SI-SNR) to specifically gauge noise-related distortion; and Non-Intrusive Speech Quality Assessment (NISQA-MOS) for reference-free estimation of perceptual speech quality.

### 4.2 Hyperparameter and Configuration

The training of NDSI-BWE is completed with carefully chosen hyperparameters. Learning rate is initialized with  $2 \times 10^{-4}$  with exponential decay after each epoch with a decay factor of 0.999. AdamW optimizer with B1 = 0.8, B2 = 0.99, and a weight decay of 0.01 are used for stable convergence. We use a batch size of 16 to balance between computational efficiency and memory utilization. All models are trained for a total of 50 epochs. We use four NVIDIA RTX 4090 GPUs and Intel(R) Xeon(R)

Silver 4310 CPUs (2.10 GHz) as a computational platform. For distributed training and potential scalability, we use the NCCL backend and TCP initialization. We use an Anaconda virtual environment with Python 3.9.21, PyTorch 2.0.0+cu118, TorchAudio 0.15.0+cu118, Torchvision 0.15.0+cu118, and CUDA Toolkit 11.8.0.

### 4.3 Dataset and Preprocessing

We use the CSTR VCTK Corpus (v0.92) (Yamagishi et al., 2019), comprising 110 multi-accent native English speakers. There are in total 400 utterances for each speakers with sampling rate of 16 and 48 KHz. Precomputed silence intervals (+/- 0.1s padding) are loaded from vctk-silences.0.92.txt and each FLAC file is loaded at 48kHz mono channel, then trimmed to its annotated silence region plus padding. A custom *Dataset class* caches audio for efficiency. The low rate input is simulated by downsampling to lower sampling rates, then upsampling back to the original sampling rate by sinc interpolation. For spectral feature extraction, we extract log-magnitude and phase by computing STFT. The generated high frequency spectrograms are converted back to audio signals by inverse STFT.

SL	MPD	MRAD	MRPD	MRLD	MSDFA	LSD	STOI	PESQ	SNR	N-MOS
1	✗	✗	✓	✗	✓	1.22	0.89	2.05	9.47	2.32
2	✗	✗	✗	✓	✓	1.20	0.85	1.55	7.47	3.58
3	✗	✓	✓	✗	✗	1.11	0.86	1.61	7.87	4.07
4	✗	✓	✗	✓	✗	1.09	0.86	1.65	8.42	4.08
5	✗	✓	✓	✓	✗	1.06	0.85	1.58	7.78	4.14
6	✗	✓	✓	✓	✓	1.10	0.87	1.66	8.11	4.29
Evaluating MPD with our proposed discriminators										
7	✓	✗	✗	✓	✗	1.23	0.85	1.53	6.95	3.58
8	✓	✗	✗	✓	✓	1.04	0.85	1.55	7.15	3.65
9	✓	✗	✗	✗	✓	1.24	0.85	1.52	7.08	3.79
10	✓	✓	✓	✗	✗	1.11	0.85	1.56	6.68	4.18
Comparison of parameters among MPD and our proposed discriminators										
11	22M	600.2k	600.2k	235.5k	247.7k					

Table 1: Ablation study on discriminators with their sizes for 2→16 kHz range. Here, N-MOS = NISQA-MOS and SNR = SI-SNR. Our MRLD + MSDFA in row ⑥ has in total 40x smaller parameters (22M vs 483.2k) compared to MPD in row ⑩ with better performance.

### 4.4 Discriminator Ablation Study

Table 1 represents the ablation results reported based on five objective evaluation metrics sorted by increasing NISQA-MOS for 2→16 kHz range.

**Row ①:** When we only use MRPD (phase) and MSDFA (fractal dynamics), the model receives feedback on fine-grained periodicity and long-range temporal self-similarity, resulting in the poorest performance (NISQA-MOS = 2.302). However, a higher SI-SNR indicates that the gener-

ator can generate phase-consistent results without generating natural-sounding envelopes.

**Row ② and ③:** MRLD (deterministic chaos) and MSDFA show an improved performance (NISQA-MOS = 3.588) as MRLD encourages realistic chaos, but without amplitude cues, the performance is lower. Using MRAD and MRPD in row ③, we obtain NISQA-MOS = 4.079 because we have both magnitude and phase cues. MRAD enforces the correct amplitude distributions, and MRPD aligns the notorious phase relationships. These combinations also score significantly higher in LSD (1.1138) and PESQ (1.6179). These results show us the efficacy of the MRAD and MRPD and make them “indispensable” in our design choice.

**Row ④ and ⑤:** We use MRLD instead of MRPD along with MRAD. This combination performs on par with MRAD and MRPD, as both phase and Lyapunov exponents capture two different types of deterministic chaos. Once again, when we use both MRLD and MRPD along with MRAD, we get an increase in NISQA-MOS to 4.14 from 4.08, which confirms the necessity of MRLD in capturing deterministic chaos rather than MRPD.

**Row ⑥:** We give fractal analysis feedback to the generator by MSDFA along with MRLD, MRPD, and MRAD. These combined features provide strong cues to the generator, which results in significant boosts to NISQA-MOS from 4.14 to 4.29. Therefore, this set of combinations is used in our proposed NDSI-BWE architecture.

#### 4.5 Comparison with MPD

As SOTA models (Lu et al., 2024b,a) use MPD, we compare the performance of our proposed MRLD + MSDFA with MPD in Row ⑦ to ⑩ of Table 1.

**Row ⑩:** The combination of MPD + MRPD + MRAD gives NISQA-MOS of 4.18, which is lower than our proposed combinations of MRLD + MSDFA + MRAD + MRPD in Row ⑥. This statement also holds for other metrics as well. As MRAD + MRPD is common in both cases, this proves that the MRLD + MSDFA performs better than MPD alone. Moreover, we are getting better performance with only 483.2k parameters in total for MRLD + MSDFA, compared to 22M parameters of MPD. This is a significant finding as our MRLD + MSDFA gives better performance compared to MPD with 40x smaller parameters (22M vs 483.2k). This will provide a stepping stone for smaller models in edge devices without sacrificing performance.

#### 4.6 Generator Architecture Ablation Study

To determine the optimal generator configuration, we performed three systematic ablations on core block selection, inter-stream connectivity, network depth, and MLP expansion ratio. The results are summarized in Table 2 for 2→16 kHz range.

**Core Block Selection:** We consider two blocks: ConvNeXt and ConformerNeXt. The reason for choosing ConvNeXt is that we want to demonstrate the better performance of our ConformerNeXt over the SOTA ConvNext (Lu et al., 2024b,a). We separately use a total of 16 ConvNext (denoted by ConvNeXt<sub>16</sub> in row ①) and ConformerNeXt (denoted by ConformerNeXt<sub>16</sub> in row ②). The row ② achieves the highest NISQA-MOS of 4.44, a +0.13 gain over ConvNeXt in row ①, along with improvements in LSD (1.10 vs 1.12), STOI (0.87 vs 0.86), and PESQ (1.70 vs 1.63). In this way, we find out the supremacy of the ConformerNeXt over ConvNeXt as a core block.

**Inter-Stream Connectivity:** We compare linear and Lattice Net for coupling magnitude and phase streams. Lattice Net in row ④ consistently outperforms the linear stream in row ③ in terms of all six metrics. Therefore, we use Lattice Net as a cross-stream interaction for its superior controlled mixing of amplitude and phase stream via learnable scalars’ gating mechanism (see Section 3.1).

**Depth and Head Count:** After getting the best core block and cross-connection scheme, we try to optimize the number of ConformerNeXt and head count in the generator. Reducing from 16 to 4 ConformerNeXt blocks (row ② vs row ④) yields a compact model with 7x reduction in size with compromising a small performance but still better/similar to SOTA models (Lu et al., 2024b,a) in Table 3. We further evaluated multi-head self-attention by reducing from 8 to 4 heads (row ⑤), leading to a minor NISQA-MOS drop (4.25 vs 4.29) compared to row ②. We also test the hidden dimension of the linear network with one-fourth (row ⑥), which degrades NISQA-MOS to 3.60.

#### 4.7 Making the Discriminator Efficient

In this section, we explain how we make our discriminators small yet efficient in terms of all six metrics. The performance of our generator is highly correlated with the numbers of scales or resolutions used in the discriminators. In rows ① to ④ of Table 2, we use three windows or scales to calculate features from three different resolutions. However, when we increase the number of scales to 5, the

SL	Architecture	Size	Discriminators	H	LSD ↓	STOI ↑	PESQ ↑	SI-SDR ↑	SI-SNR ↑	NISQA-MOS ↑
1	ConvNeXt <sub>16</sub>	106.34M	[MRLD + MSDFA + MRA/PD]x3	-	1.12	0.86	1.63	7.89	7.88	4.31
2	ConformerNeXt <sub>16</sub>	223.2M	[MRLD + MSDFA + MRA/PD]x3	8	1.10	0.87	1.70	7.93	7.90	4.44
3	ConformerNeXt <sub>4</sub> , Linear	64.23M	[MRLD + MSDFA + MRA/PD]x3	8	1.12	0.86	1.57	7.66	7.62	4.32
4	ConformerNeXt <sub>4</sub>	32.7M	[MRLD + MSDFA + MRA/PD]x3	8	1.09	0.87	1.71	8.56	8.54	4.03
5	ConformerNeXt <sub>4</sub>	33.5M	[DSC(MRLD+MSDFA) + MRA/PD]x5	4	1.10	0.87	1.67	8.24	8.20	4.25
6	ConformerNeXt <sub>4</sub> , MLP /4	16.67M	[DSC(MRLD+MSDFA+MRA/PD)]x5	4	1.12	0.87	1.68	8.01	7.98	3.60
7	ConformerNeXt <sub>4</sub> (Proposed)	33.5M	[DSC(MRLD + MSDFA) + MRA/PD]x5	8	1.10	0.87	1.66	8.14	8.11	4.29

Table 2: Generator architecture ablation study for 2→16 kHz range. SI-SNR and SI-SDR use dB unit. H = number of attention heads in the multi-head self attention of the ConformerNeXt block.

feature maps capture more fine-grained as well as coarse-grained temporal patterns to provide better performance, which is shown in rows ⑤ to ⑦ of Table 2. Due to the larger scale of 5, though it might take slightly more train time due to calculate more features, our discriminators can guide the generator for more faithful reconstruction without any increase in the number of parameters.

Moreover, we use Depth-wise Separable Convolution (DSC) in our discriminators to shrink their sizes. In rows ① to ④ of Table 2, we use normal convolution but in rows ⑤ to ⑦, we try with different combinations of DSC with our discriminators. For example, in rows ⑤ and ⑦: DSC in MRLD and MSDFA + normal convolution in MRAD and MRPD; in row ⑥: DSC in all MRLD, MSDFA, MRAD and MRPD.

We implement DSC by factorizing standard convolutions into  $K \times 1$  group-wise depthwise steps, followed by  $1 \times 1$  pointwise convolutions for cross-channel fusion. This results in a  $20\times$  reduction in the number of parameters and reduces the computational complexity from  $\mathcal{O}(KC_{in}C_{out})$  to  $\mathcal{O}(KC_{in} + C_{in}C_{out})$ . This structural simplification significantly lowers the parameter count and improves computational efficiency, shown in Table 5.

**Final Design:** Based on all these ablations, our final generator employs a total of 4 ConformerNeXt blocks (each with 8 heads and linear projection hidden dimension  $\times 4$ ), interconnected via Lattice Net, resolution of 5 together with DSC in MRLD and MSDFA + normal convolution in MRAD and MRPD (row ⑦). This configuration achieves the best trade-off between perceptual quality (NISQA-MOS = 4.29), computational efficiency, and parameter compactness ( $\approx 33.5$  M parameters).

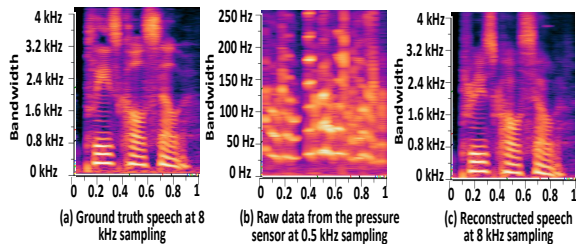


Figure 3: Dummy.

## 4.8 Comparative Analysis with Baselines

Table 3 compares how our proposed NDSI-BWE performs against three baseline models - EBEN (Hauret et al., 2023), AERO (Mandel et al., 2023), AP-BWE (Lu et al., 2024a), NU-Wave (Lee and Han, 2021), and MS-BWE (Lu et al., 2024b) - over three extension ranges (4→16 kHz, 8→16 kHz and 16→48 kHz). EBEN is a Pseudo Quadrature Mirror Filter-based model, AERO is a complex-valued model, NU-Wave is a diffusion model, AP-BWE and MS-BWE are dual-stream for amplitude and phase prediction models.

Compared to unprocessed speech (downsampled and sinc interpolated), NDSI-BWE significantly does a 3x reduction in LSD, 1.72x increase in STOI, 2.17x increase in PESQ, and 1.51x increase in NISQA-MOS for 4→16 kHz. Table 3 also indicates that AP-BWE and MS-BWE are the two best-performing models. Compared with these two recent baselines, the proposed NDSI-BWE exceeds in LSD, PESQ, NISQA-MOS, and STOI for all three frequency ranges. However, NDSI-BWE gives similar performance for SI-SDR and SI-SNR compared to AP-BWE and MS-BWE. Please note that LSD is a measure for over-smoothing, and NISQA-MOS, PESQ, and STOI are the measures of perceptual audio quality. Our model outperforms the two recent baselines - AP-BWE and MS-BWE - for these perceptual and over-smoothing metrics with almost 2.18x and 1.28x fewer parameters, respectively (72M vs 43M vs 33M). Our NDSI-BWE is benefiting from the explicit chaotic feature extraction in amplitude and phase domains, successfully avoiding the compensation effects between amplitude and phase. It is also an indication that our approach of chaotic modeling using chaos-informed discriminators is out-performing other non-linear discriminators, such as MPD, with fewer parameters (see Section 4.5). This finding is a stepping stone for adopting chaos-informed discriminators in the existing generative models to capture both the fine-grained spectral details and deterministic chaos, resulting in less over-smoothed or more perceptually natural sounds.

Method	Size (M)	LSD			STOI			PESQ			SI-SDR			SI-SNR			NISQA-MOS		
		4-16	8-16	16-48	4-16	8-16	16-48	4-16	8-16	16-48	4-16	8-16	16-48	4-16	8-16	16-48	4-16	8-16	16-48
Unprocessed	-	3.27	2.27	2.85	0.55	0.61	0.61	1.15	1.51	1.41	-11.03	-8.07	-6.07	-10.53	-7.62	-5.63	2.79	3.67	4.43
NU-Wave (2021)	-																		
EBEN (2023)	29.7																		
AERO (2023)	NA																		
AP-BWE (2024)	72	0.96	0.74	0.75	0.94	0.99	0.99	2.55	3.69	3.72	13.42	18.26	20.86	13.35	18.07	20.74	3.86	3.97	4.49
MS-BWE (2024)	43		0.72	0.73															
NDSI-BWE	33.5	0.98	0.79	0.79	0.95	0.99	0.99	2.50	3.72	3.61	13.24	18.13	19.53	13.15	17.98	19.44	4.24	4.26	4.53

Table 3: Comparative analysis of baseline models over three extension ranges with our proposed NDSI-BWE.

#### 4.9 Study for Different Frequency Ranges

Table 4 further investigates NDSI-BWE’s performance across different frequency ranges. Overall, expanding the input frequency band generally leads to improvements across most evaluation metrics. For instance, the LSD consistently decreases as the lower bound of the input frequency increases, with the best score of 0.6531 achieved for the 24–48 kHz range, indicating better spectral reconstruction. Similarly, perceptual metrics such as PESQ and NISQA-MOS improve with wider input bands, peaking at 4.1822 and 4.5254, respectively, for the 24–48 kHz range, suggesting enhanced perceptual quality and naturalness. Temporal fidelity metrics like SI-SDR and SI-SNR also follow this trend, reaching their maximum values (23.42 dB and 23.38 dB) in the same range. Interestingly, STOI scores are high (above 0.99) for mid-to-high frequency inputs (e.g., 12–48 and 24–48 kHz), implying strong speech intelligibility preservation when higher frequency content is available. These results confirm that the model leverages broader frequency context to significantly enhance both objective and perceptual reconstruction quality.

Freq. range	LSD	STOI	PESQ	SI-SDR	SI-SNR	NISQA-MOS
2-16 kHz	1.1068	0.8739	1.66	8.1487	8.118	4.2979
2-48 kHz	1.21	0.8526	1.1836	6.963	6.9662	3.9987
4-48 kHz	1.099	0.933	1.4921	12.045	11.99	4.2294
8-48 kHz	1.092	0.933	1.506	12.39	12.33	3.975
12-48 kHz	0.873	0.9976	3.1253	17.085	16.95	4.4854
24-48 kHz	0.6531	0.9989	4.1822	23.42	23.38	4.5254

Table 4: Performance of NDSI-BWE over different frequency ranges.

#### 4.10 Computational Complexity

Table 5 investigates the computational complexity and real-time performance of NDSI-BWE using Multiply-Accumulate Operations (MACs), Floating Point Operations per seconds (FLOPs), and Real-Time Factor (RTF) across two different frequency ranges. Due to the optimization of the generator and discriminators (see Sections 4.6 and 4.7), NDSI-BWE uses 0.5x fewer parameters, MACs, and FLOPs compared to AP-BWE, while maintaining superior perceptual quality as shown by NISQA-MOS scores in Table 3. NDSI-BWE also has a low RTF (0.0025x), which indicates that

it can be implemented effectively in applications where real-time audio generation is required, such as video streaming services. Moreover, due to the half number of parameters, NDSI-BWE is more suitable for resource-constrained edge devices compared to AP-BWE.

Model	Fq. Range	Params (M)	MACs (M)	FLOPs (M)	RTF (GPU)
AP-BWE	4-16 kHz	72.07	14236.65	28473.31	0.0023x
AP-BWE	16-48 kHz	72.07	14236.65	28473.31	0.0025x
NDSI-BWE	4-16 kHz	33.74	6790.86	13581.73	0.0025x
NDSI-BWE	16-48 kHz	33.74	6790.86	13581.73	0.0028x

Table 5: Computational complexity of NDSI-BWE. The hardware configuration is provided in Section 4.2.

## 5 Conclusion

Both in subjective and objective results demonstrate that NDSI-BWE significantly improves the perceptual quality of the reconstructed speech across different frequency bands. The key innovations of our paper lies in the introduction of two novel chaos and non-linear dynamical systems inspired and two other discriminators each focusing a unique aspect of frequency patterns. By explicit modeling of deterministic chaos, fractal cues, periodicity, amplitude dynamics, and phase transitions the discriminators provide subtle nuances that contemporary discriminators usually overlook. This multi-discriminators supervises to produce enhanced, natural sounding audios by reducing perceptual artifacts and successful inpainting of high frequency components. Due to usage of depth-wise separable convolutions, the higher performance achieved without sacrificing performances. Our proposed ConformerNeXt successfully combine the local temporal modeling capacity of convolution with Transformers long-range dependencies to reproduce faithful audios. Additionally, due to the reduced number of parameters due to the usage of Depth-wise separable convolutions, this performance is achieved with 05x reduced number of parameters. This makes NDSI-BWE an ideal candidate for deployment in resource-constrained real-time applications.

## 6 Limitations and Future Work

Our current works only focus on one rather than multiple datasets in noise-free settings. However, the real-world environments often has noises that challenges the robustness of this type of models. Proposed NDSI-BWE performs well for English language VCTK dataset. In multi-lingual, cross-speaker, and low-resource settings the generalization ability is not tested. Though discriminators are highly parameter-efficient, the overall training and inference time is slightly more because of large number features, controlled cross-stream mixing, and nonlinear calculations involved.

## 7 Ethical Considerations

While the intention of designing NDSI-BWE model is for frequency restoration research purposes, it can be misused for potential secret evading, impersonation, or deepfake audio generation. This model has the potential for severe privacy and security risks. To avoid these, we have to be very careful to ensure transparency, protect consent, and always follow guidelines.

## References

- Yubing Cao, Yongming Li, Liejun Wang, and Yinfeng Yu. 2024. Vnet: A gan-based multi-tier discriminator network for speech synthesis vocoders. In *2024 IEEE International Conference on Systems, Man, and Cybernetics (SMC)*, pages 4384–4389. IEEE.
- Chris Donahue, Julian McAuley, and Miller Puckette. 2018. Adversarial audio synthesis. *arXiv preprint arXiv:1802.04208*.
- Anmol Gulati, James Qin, Chung-Cheng Chiu, Niki Parmar, Yu Zhang, Jiahui Yu, Wei Han, Shibo Wang, Zhengdong Zhang, Yonghui Wu, and Ruoming Pang. 2020. **Conformer: Convolution-augmented transformer for speech recognition**. In *Interspeech 2020*, pages 5036–5040.
- Julien Hauret, Thomas Joubaud, Véronique Zimpfer, and Éric Bavu. 2023. **Eben: Extreme bandwidth extension network applied to speech signals captured with noise-resilient body-conduction microphones**. In *ICASSP 2023 - 2023 IEEE International Conference on Acoustics, Speech and Signal Processing (ICASSP)*, pages 1–5. IEEE.
- Kundan Kumar, Rithesh Kumar, Thibault De Boissiere, Lucas Gestin, Wei Zhen Teoh, Jose Sotelo, Alexandre De Brebisson, Yoshua Bengio, and Aaron C Courville. 2019. Melgan: Generative adversarial networks for conditional waveform synthesis. *Advances in neural information processing systems*, 32.
- Junhyeok Lee and Seungu Han. 2021. **Nu-wave: A diffusion probabilistic model for neural audio upsampling**. In *Interspeech 2021*, pages 1634–1638.
- Max Little, Patrick Mcsharry, Stephen Roberts, Declan Costello, and Irene Moroz. 2007. Exploiting nonlinear recurrence and fractal scaling properties for voice disorder detection. *Nature Precedings*, pages 1–1.
- Zhuang Liu, Hanzi Mao, Chao-Yuan Wu, Christoph Feichtenhofer, Trevor Darrell, and Saining Xie. 2022. **A convnet for the 2020s**. In *Proceedings of the IEEE/CVF conference on computer vision and pattern recognition*, pages 11976–11986.
- Ye-Xin Lu, Yang Ai, Hui-Peng Du, and Zhen-Hua Ling. 2024a. Towards high-quality and efficient speech bandwidth extension with parallel amplitude and phase prediction. *IEEE/ACM Transactions on Audio, Speech, and Language Processing*.
- Ye-Xin Lu, Yang Ai, Zheng-Yan Sheng, and Zhen-Hua Ling. 2024b. Multi-stage speech bandwidth extension with flexible sampling rate control. *arXiv preprint arXiv:2406.02250*.
- Xiaotong Luo, Yuan Xie, Yulun Zhang, Yanyun Qu, Cuihua Li, and Yun Fu. 2020. **LatticeNet: Towards Lightweight Image Super-Resolution with Lattice Block**. In Andrea Vedaldi, Horst Bischof, Thomas Brox, and Jan-Michael Frahm, editors, *Computer Vision – ECCV 2020 (Lecture Notes in Computer Science, vol 12367)*, pages 272–289. Springer, Cham.
- Moshe Mandel, Or Tal, and Yossi Adi. 2023. Aero: Audio super resolution in the spectral domain. In *ICASSP 2023-2023 IEEE International Conference on Acoustics, Speech and Signal Processing (ICASSP)*, pages 1–5. IEEE.
- V.I. Oseledec. 1968. A multiplicative ergodic theorem: Lyapunov characteristic numbers for dynamical systems. *Trans. Moscow Math. Soc.*, 19:197–231.
- Qiao Tian, Yi Chen, Zewang Zhang, Heng Lu, Linghui Chen, Lei Xie, and Shan Liu. 2020. Tfgan: Time and frequency domain based generative adversarial network for high-fidelity speech synthesis. *arXiv preprint arXiv:2011.12206*.
- Alan Wolf, J. B. Swift, Harry L. Swinney, and John A. Vastano. 1985. Determining lyapunov exponents from a time series. *Physica D: Nonlinear Phenomena*, 16(3):285–317.
- Junichi Yamagishi, Christophe Veaux, Kirsten MacDonald, and 1 others. 2019. Cstr vctk corpus: English multi-speaker corpus for cstr voice cloning toolkit (version 0.92). *University of Edinburgh. The Centre for Speech Technology Research (CSTR)*, pages 271–350.
- Dacheng Yin, Chong Luo, Zhiwei Xiong, and Wenjun Zeng. 2020. Phasen: A phase-and-harmonics-aware speech enhancement network. In *Proceedings of the AAAI Conference on Artificial Intelligence*, volume 34, pages 9458–9465.